JOURNAL OF MATERIALS SCIENCE 32 (1997) 67–72

Stress corrosion cracking of pyrotherm reformer tube for steam-reforming hydrogen production

T. C. CHOU, W. HUANG, R. PACIEJ
BOC Group Technical Centre, 100 Mountain Ave., Murray Hill, NJ 07974 USA

A section of Pyrotherm G 25/35 Nb reformer tube was rupture-failed in a steam-reforming hydrogen plant and analysed to identify the causes of failure. Examination of the internal surface of the pipe indicated signs of heterogeneous corrosion attack in localized areas near to the primary crack site. Some of these areas were associated with fissures, although they did not penetrate through the pipe wall. Measurement of the pipe wall thickness revealed that fair amounts of the material had been consumed by corrosion. Cross-sectional examination of the dissected pipe in areas showing signs of corrosion attack and fissures revealed the presence of radial macrocracks, originating from the internal surface, and numerous microcracks in the pipe interior. Most microcracks were formed along the grain boundaries of the spin-cast microstructure. Further examination of the macrocracked surfaces revealed the presence of a granular microstructure, indicative of a brittle failure mode. Based on the characteristics exhibited by the macrocracking, the rupture failure of the reformer tube is attributed to stress corrosion cracking (SCC). The SCC is believed to be produced through synergistic reactions amongst sulfur-containing derivatives in the natural gas (feedstock), hydrogen and superheated steam in the processed gases under a mechanically-stressed environment. The presence of the mechanical stress is attributed to the bending of the pipe caused by improper suspension design.

1. Introduction

Stress corrosion cracking (SCC) has been the subject of a number of reviews in recent years [1–7]. The phenomenon of SCC can be defined as the occurrence of macroscopic brittle fracture of a normally ductile metal due to the combined actions of stress and local environment [6]. A classical example of SCC is stainless steel in chloride environments [7]. Amongst many attributes of SCC, two important characteristics are noteworthy: (1) the environment need not be chemically aggressive to result in a high general dissolution rate, and (2) the roles and effects of anodic dissolution and hydrogen absorption in cracking are generally difficult to differentiate. SCC has been identified to occur in a number of material systems, including ferritic steels, stainless steels, high-strength steel, and titanium, magnesium and aluminium alloys. The intent of this paper is to present a case study on the rupture failure of a high-alloy stainless steel in a hydrogen production environment.

Hydrogen can be found in the molecular structures of hydrocarbons, proteins, amino acids and in DNA and RNA [8]. It is considered as a utility chemical and is widely used in a multitude of industries including petroleum refinery, chemical production, food processing and steel making. In these industries, hydrogen is employed as a reactive agent for the following applications: (1) hydro-cracking of higher molecular weight hydrocarbons, (2) synthesizing ammonia and methanol, (3) hydro-treating unsaturated oils/fats, (4) converting S to H_2S for further removal, and (5) serving as a reducing atmosphere for heat treatment.

Hydrogen is mainly produced via the following technologies: (1) steam reforming of natural gas, (2) partial oxidation of heavy oils, (3) coal gasification, and (4) electrolysis of water. This study concerns the rupture failure of a reformer tube (also known as a catalyst tube) used in a steam reforming process. To the best of our knowledge, rupture failure occurs periodically to the reformer tubes during hydrogen production, but has been rarely reported in materials science and engineering journals. To facilitate understanding the nature of rupture failure of the reformer tube, brief background information is provided on the chemical process and material characteristics. Detailed technical information pertaining to steam-reforming processing for hydrogen production can be found elsewhere [8–10].

The reformer tube in question was exposed to superheated steam and sulfur-containing natural gas which was piped through a heater and a hydrogen-desulfurizer. The gases were reacted in the presence of catalysts in a number of vertically-oriented reformer tubes which were aligned in parallel and housed in a top-fired reformer furnace. The chemical reaction

0022–2461 © *1997 Chapman & Hall*

taking place at this stage is an endothermic one and can be described as $CH_4 + H_2O \rightarrow 3H_2 + CO$. The CO gas undergoes an exothermic shift reaction $CO + H_2O \rightarrow H_2 + CO_2$ for conversion into H_2 [9]. The hydrogen gas is then separated from CO_2 and further purified by adsorption techniques [8, 9].

Historically, centricast Cr–Ni–Fe heat-resistant alloy steels (Alloy Castings Institute HK and HU types) and preferred to wrought alloys for use in reformer tubing [11]. This stems largely from a combination of economic reasons and the availability of longer lengths of centricast tube. To date, Pyrotherm alloys or Paralloys have been widely used in the last 15 years for reformer tubes in reformer furnaces. These types of heat-resistant steels are easily welded using metal arc or inert gas shielded arc welding processes using matching filler materials. The pipe involved in this study was a Pyrotherm G 25/35 Nb alloy. Under normal operating conditions, the pipe was operated at pressures no greater than 20 barg and temperature ranging from 450–800 °C. The pipe was bent, rather than straight, after plant commissioning for a period of time due to the combined effects of high-temperature creep, thermal expansion and mechanical suspension design of the reformer furnace. The pipe failed after a service life of approximately 7000 h. Reformer pipes operated under the aforementioned conditions are expected to have life expectancy of at least 10–11 years. The typical design life time for reformer tubes at their maximum operating temperature is 100 000 h, based on selected wall thickness and creep strength data deduced from creep-rupture tests [9, 10].

2. Material description and experimental procedures

The Pyrotherm G 25/35 Nb reformer tube has the following chemical compositions (in wt %): Ni = 35.5–37, Cr = 25.5–27, Nb = 1.3–1.7, Mn = 0.5–1.3, Si = 1.0–1.5, C = 0.35–0.45, S = 0.03 max, P = 0.045 max, Fe balance. The purpose of adding Nb is to increase the creep strength of the material by forming primary Nb-carbide in the as-cast structure and secondary Nb-carbide during the service stage at high temperatures. Based on the composition, the material can be classified as a cast austenitic stainless steel (HP). The pipe was manufactured by Pose-Marre Edelstahlwerk G.M.B.H. using spin casting and inside drilled without any post-manufacturing heat treatment. In the as-cast condition, chromium carbides ($Cr_{23}C_6$ and Cr_7C_3) and niobium carbide (NbC) were formed in the grain matrix as well as on the grain boundaries [12]. The dimensions of the pipe were 121.1 (O.D.)/101.6 (I.D.) × 8884.2 (length), in mm. This translates to a pipe wall thickness of about 10 mm.

The ruptured section was separated from the whole pipe and photographed as shown in Fig. 1(a). The primary evidence of rupture, the formation of longitudinal cracks of about a 4 mm width and 15 cm in length, was destroyed by grinding in an attempted welding repair. As a result, the primary cracks featured like an open slot which was denoted by arrow A in Fig. 1(a). During the repair, a new crack [denoted by arrow B in Fig. 1(a)] was formed as a result of heating at 1100 °C.

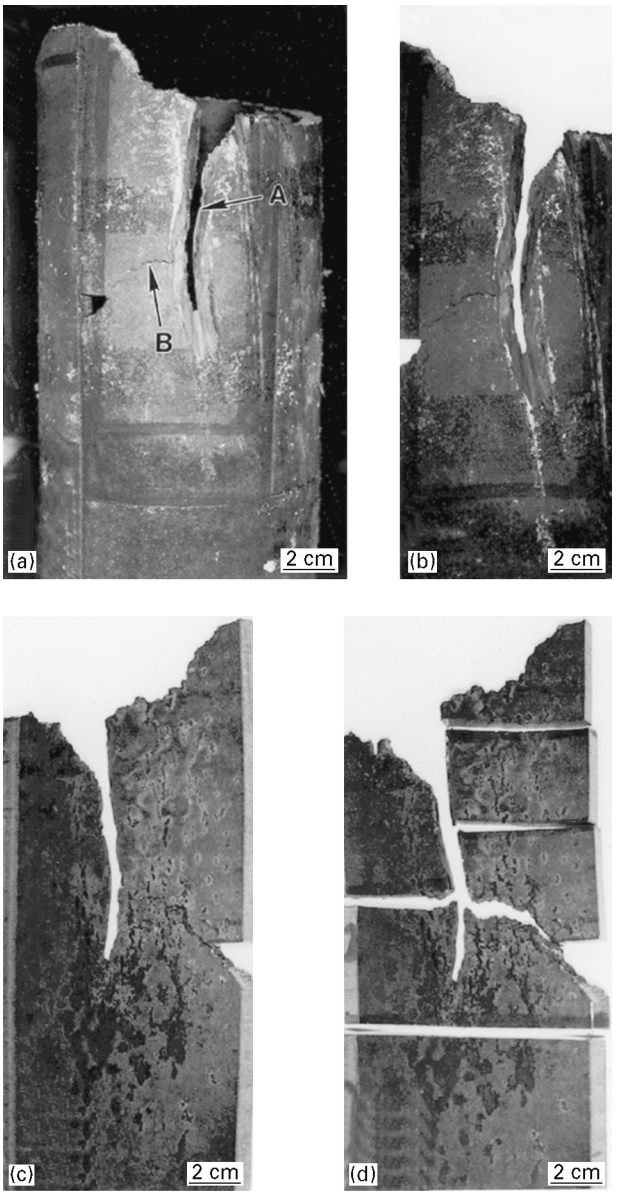

Figure 1 Optical photographs showing the characteristics of (a) the sectional ruptured pipe and (b) the external and (c) the internal surface of the rectangular sample piece. The locations of various samples dissected from the rectangular piece are indicated in (d).

To proceed with failure analysis, a rectangular piece [see Figs. 1(b and c)] was isolated from the sectioned pipe and further dissected into a number of samples [see Fig. 1(d)] in the neighbourhood of the primary crack site. For comparison purposes, samples were also dissected from areas 180° away from the primary crack site, which were free of cracking. The dissected samples were examined in both plane view and cross-section view by optical microscopy and scanning electron microscopy (SEM) with EDS (energy dispersive) X-ray spectroscopy. Metallurgical samples underwent microstructural characterization using an SEM with EDS analysis and X-ray mapping facilities. Additionally, X-ray photoelectron spectroscopy (XPS) was employed to characterize the chemistry of the cracked surfaces and grain boundaries. To verify whether the pipe material with its associated microstructure is

susceptible to SCC, the ASTM G 108 standard test method for electrochemical reactivation (EPR) for detecting sensitization of stainless steels was employed. Detailed experimental procedures for the EPR test can be found in reference [13].

3. Experimental results and discussion

3.1. Visual observation

On the internal pipe surface, numerous areas were noted to exhibit signs of heterogeneous corrosion attack in the neighbourhood of the primary crack site. These areas exhibited a brownish colour with some of them associated with either continuous or discontinuous fissures, denoted by arrows in Fig. 2(a). By contrast, signs of heterogeneous corrosion attacks were not observed either in the remote areas of the internal surface or on the external surface. The external pipe surface was covered by an oxide scale and exhibited a blackish colour.

Cross-sectional views (along the transverse/radial direction) of the dissected pipe in areas containing the fissures revealed the presence of a few radial cracks [Fig. 2(b)], originating from the internal surface and propagating towards the external surface. These fissures have not yet evolved into through-wall-thickness cracks. They developed along both the longitudinal and radial directions of the pipe with a tendency to bridge together forming continuous cracks. Given enough time, these cracks are expected to go through the wall thickness and rupture the pipe.

The thickness of the pipe wall was measured at different points using a micrometer. The wall thickness nearby the primary crack site was much thinner, about 8.3 mm, than the specified nominal wall thickness of 10 mm. This indicates the consumption of pipe material through corrosion/erosion by the processed gases. By comparison, the wall thicknesses in areas remote from the primary crack site ranged from 9.5 mm (90° away) to 10.1 mm (180° away).

3.2 Microstructural characterization and XPS analysis

Metallographic examination of the pipe, along the transverse direction, in areas near to the primary crack site revealed the presence of numerous internal microcracks. Fig. 3(a and b) show optical photographs featuring the characteristics of microcrack-bearing

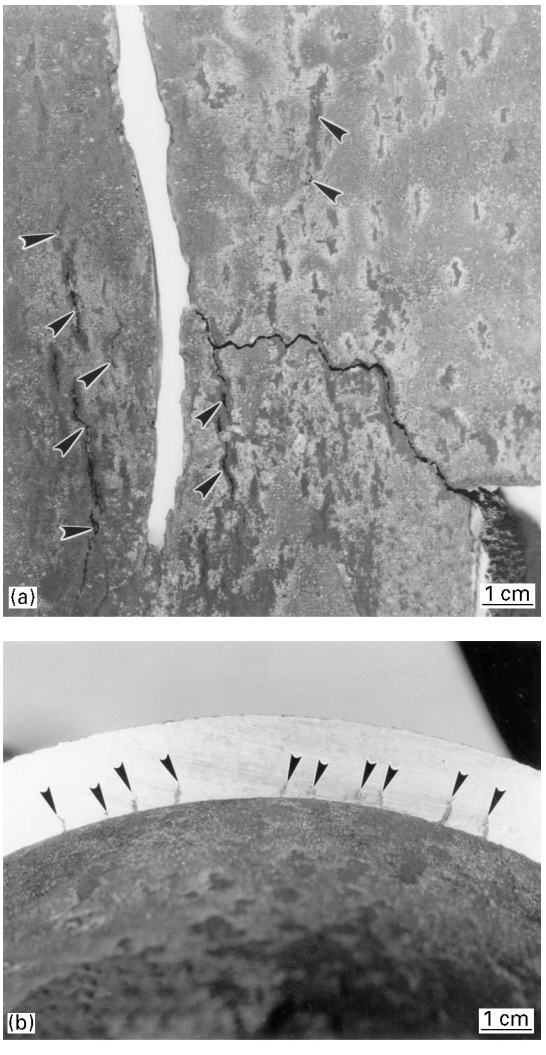

Figure 2 Optical photographs showing (a) the signs of heterogeneous corrosion attack and (b) the presence of radial cracks. The presence of fissures is evident in areas denoted by arrows in (a).

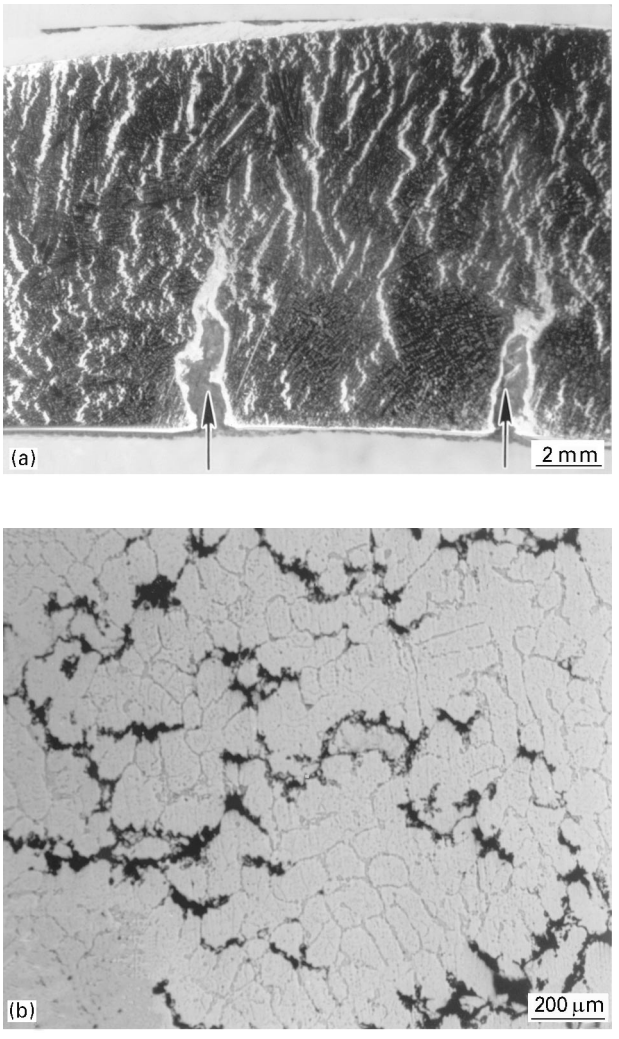

Figure 3 Optical photographs showing the characteristics of internal microcracking at (a) low and (b) high magnifications. Indicated in (a) by arrows are radial macrocracks originated from the pipe internal surface.

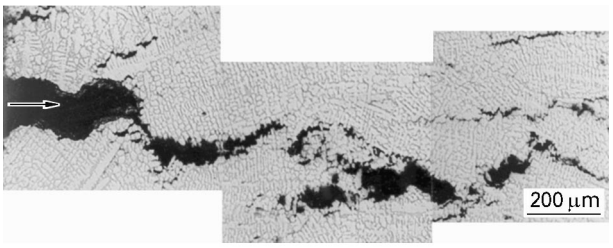

Figure 4 Optical photographs showing the presence of an originating surface macrocrack (denoted by an arrow on left) and internal microcracks.

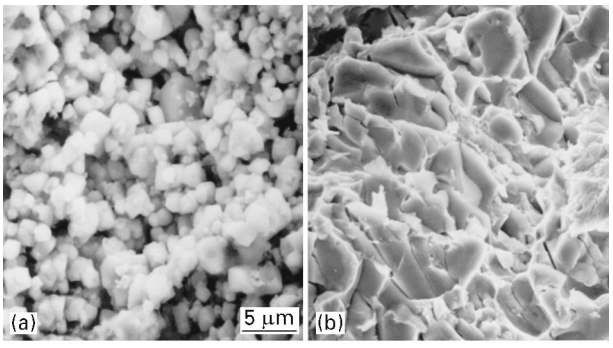

Figure 5 SEM photomicrographs showing (a) the typical granular microstructure observed on macrocracked surfaces and (b) the typical microstructure of cleavage fracture on *ex-situ* fractured surfaces.

surfaces. As is shown in Fig. 3(b), cellular grain boundaries resulting from the spin casting are clearly visible in the microstructure. The microcracks were formed primarily along the grain boundaries. In all the samples examined, creep voids that are characteristic of most creep rupture failures were not observed. Typical photomicrographs showing the features of an originating surface macrocrack as well as branching-out internal microcracks are presented in Fig. 4. Close examination of the macrocracked surfaces revealed the presence of a granular microstructure [Fig. 5(a)], indicative of a brittle failure mode. By contrast, the microstructure of *ex-situ* fractured surfaces in areas remote from the cracks revealed a transgranular failure mode showing primarily cleavage facets [Fig. 5(b)].

According to the experimental evidence presented above, the mechanism responsible for the cracking of the reformer tube is attributable to stress corrosion cracking (SCC). The possibility of creep rupture failure was dismissed based on the fact that the operating temperature and pressure of the pipe were well below the designed 100 000 h creep rupture strength–temperature profile for the material. More importantly, creep voids due to dislocation pile-up were not observed in the vicinity of the cracks.

In order for SCC to serve as a viable failure mechanism, in principle, the material needs to be exposed to a corrosive environment under stressed conditions. In the subject reactor pipe, the processed gases comprised sulfur-containing natural gas, superheated steam, H_2, CO and CO_2. Although a desulfurizer was installed in the upstream, it is possible that a few ppm levels of sulfur broke through the unit and contributed to the SCC in question. As a result sulfur-containing derivatives, hydrogen (a source for forming H_2S) and moisture reacted in a synergistic manner to serve as the corrosive environment. Under such an environment, the presence of a stress (tensile) in the material could trigger SCC. Pyrotherm alloys in the as-cast condition and containing 6, 20 and 60 wt % Ni contents have been demonstrated to be susceptible to corrosion under a hydrogen-sulfide containing and carburizing atmosphere [14]. In the present case, the species responsible for SCC is believed to be present in a mixed state containing both gaseous and condensed phases. The possibility of hydrogen embrittlement was ruled out, because the material was tested and found not to be susceptible to hydrogen embrittlement based on the studies performed by two individual material manufacturers [12, 15].

To identify the chemical species responsible for the SCC, attempts were made using XPS to analyse heterogeneously corroded areas on the pipe internal surface as well as on SCC-failed fractured surfaces as opposed to artificially-cracked surfaces. Unfortunately the XPS results were unable to distinguish the corroded areas or SCC-failed fractured to surfaces. All the surface areas examined were found to contain no sulfur but were heavily contaminated by oxygen. This is believed to have been caused by oxidation due to welding repairs performed at elevated temperatures. It is likely that the fingerprint of the corrosive species is masked by the surface oxide layer formed subsequent to the crack formation or corrosion attacks.

For comparison purposes, the materials's microstructure was examined in areas remote from the primary crack site. No internal microcracking was observed, although the material also exhibited a cellular microstructure similar to that in areas nearby the

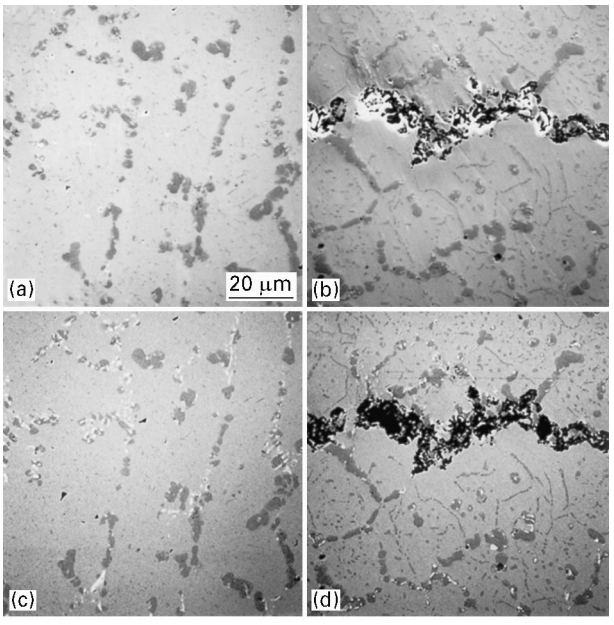

Figure 6 Electron photomicrographs showing the secondary electron images, (a) and (b), and backscattered electron images, (c) and (d), of the microstructure in areas remote from and nearby the primary crack site, respectively. Cr-enriched regions are featured by the dark-grey areas in (a), (b), (c) and (d); Nb-enriched regions are characterized by the white dotted areas in (c) and (d).

primary crack site. Typical SEM photomicrographs showing the microstructures in areas remote from and nearby the primary crack sites are presented in Fig. 6(a and b), respectively. The cellular microstructure observed in the remote areas appears to be similar to that of the as-cast pipe [12]. This suggests that the thermal energy infused into the reformer tube by the steam-reforming process was not significant enough to induce appreciable grain growth. According to the EDX microanalysis, the cellular boundaries were strongly enriched with chromium (Cr) and niobium (Nb), as compared to the grain matrix. The Cr content in segregated boundaries could reach 85 wt %, as compared to a nominal composition of 25.5–27 wt %; the Nb content reached 75 wt %, as compared to a nominal composition of 1.3–1.7 wt %. Although a quantitative WDS (wavelength dispersive spectrometry) analysis is yet to be performed, the segregation of Cr and Nb to the grain boundaries is attributed to the formation of carbides due to their highly negative Gibbs free energy of formation [16, 17]. It is important to note that Cr and Nb segregated to different regimes of the grain boundaries. The differential segregation behaviour is better contrasted in the backscattered electron photomicrographs shown in Fig. 6(c and d), and best illustrated using X-ray mapping as is shown in Fig. 7.

Segregation of Cr to grain boundaries, *in lieu* of uniform dissolution in the solid solution matrix, poses two deleterious effects to the material. From the standpoint of creep strength, the formation of Cr-carbide limits the availability of carbon to Nb for the formation of the creep strengthening phase NbC. From a corrosion standpoint the grain boundary segregation of Cr gives rise to the formation of a Cr-depletion zone nearby the boundary due to diffusion kinetics. This is highly undesirable because the low-

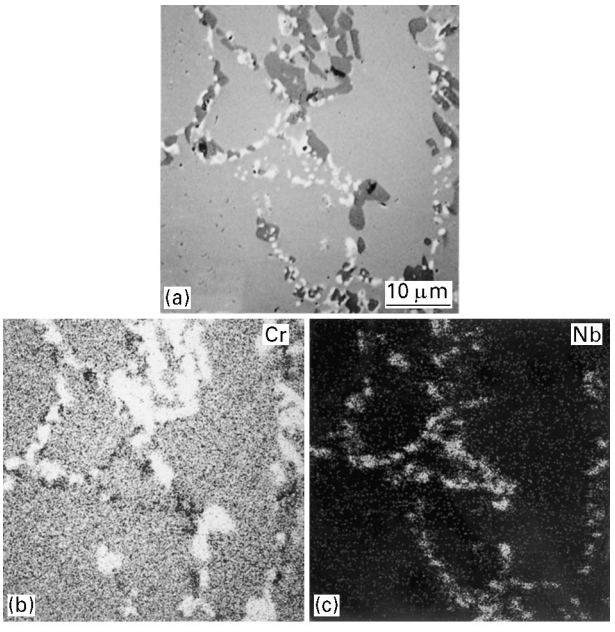

Figure 7 (a) A backscattered electron photomicrograph of X-ray maps of the corresponding area showing the differential segregation behaviour of (b) Cr and (c) Nb in the grain boundary regimes.

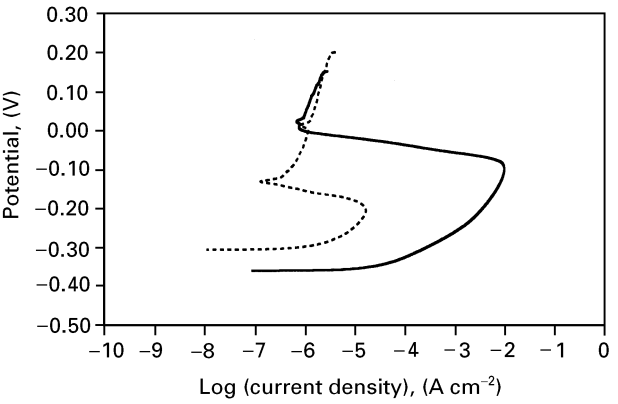

Figure 8 Electrochemical reactivation curves measured from (—) Pyrotherm G 25/35 Nb alloy and (- - -) 304 SS.

Cr-content regime is anodic to the rest of the grain [18], which is turn renders the material susceptible to SCC (or intergranular corrosion) in a corrosive environment when under stress. The mechanism for SCC in the present case is similar to that for the sensitization of stainless steel, which is effected by the segregation of Cr to the grain boundaries [18, 19]. The susceptibility of the subject pipe material of SCC was further verified by electrochemical reactivation (EPR) tests conducted (at 30 °C) in compliance with ASTM G-108. A typical EPR curve measured from the pyrotherm G alloy is displayed in Fig. 8. As a comparison, the EPR curve of a solutionized AISI 304 stainless steel which is not susceptible to intergranular corrosion is also shown in Fig. 8. It is clearly observed that the anodic current density measured from the Pyrotherm alloy was about 3 orders of magnitude higher than that from the 304 SS. The test results indicate that the Pyrotherm alloy is highly susceptible to intergranular corrosion and/or intergranular stress corrosion cracking [13].

With regard to the stress that is required to facilitate SCC, it is attributable to pipe bending caused by material creep and thermal expansion at high temperature under a constrained boundary condition. The contribution of residual stress in the pipe due to manufacturing process is believed to be minimal, because of the stress-relieving effect provided by the high-temperature process. Bending is expected to give rise to various tensile and compressive stresses at different locations of the pipe. Considering a finite plate under bending moments as an example for illustration, according to the equation $\sigma = My/I$, where σ is the bending stress, M is bending moment, y is the distance from the neutral plane, and I is the second moment of area, maximum stress is expected to occur on the free surfaces at the location with maximum deflection. In the case of a pipe, free surfaces are either the internal or external surface. In view of the fact that the internal surface suffers the most severe corrosive environment, SCC is expected to nucleate from the internal surface. Therefore, the general location of the primary crack is anticipated to be in the proximity of the bend where deflection was the greatest. This is generally in good agreement with what has been observed in the past on the rupture failures of steam-reforming reactor pipes.

As SCC is a type of chemical reaction whose reaction rate is also governed by the temperature at which the reaction takes place. Therefore, the higher temperature the pipe material encounters, the faster the kinetics of SCC. This appears to be consistent with the fact that the ruptured pipe, based on its design layout in the reformer furnace, received the most heat from the burners in the reformer. Additionally, functional capability of the nickel oxide catalysts can also affect the temperature of the material in contact. Since steam reforming of natural gas involves an endothermic reaction, the inability of catalyst due to the sulfur-poisoning can produce localized hot spots in the reformer tube.

4. Conclusions

Rupture failure of a G 25/35 Nb steam-reforming reformer tube was investigated. Examination of the pipe internal surface in areas near to the primary crack site revealed signs of heterogeneous corrosion attack in numerous areas. Some of these areas were associated with fissures, although they had not penetrated through the pipe wall. By contrast, areas remote from the primary crack sites were free of corrosion attack. Measurement of the pipe wall thickness revealed that fair amounts of the material had been consumed by corrosion. A cross-sectional examination of the pipe in areas showing signs of corrosion attack and fissures visually revealed the presence of radial macrocracks originating from the internal surface. Metallographic examination indicated the presence of numerous microcracks in the pipe interior, with some of them extending and/or branching-out from the surface macrocracks. Most microcracks were formed along the grain boundaries. Further examination of the macrocracked surfaces revealed the presence of a granular microstructure, indicative of a brittle failure mode. As a comparison, *ex-situ* fractured surfaces revealed a facet cleavage fracture pattern. Based on the characteristics of the macrocracking and microcracking phenomena, and the fact that no creep voids were observed near the rupture cracks, the rupture failure of the reformer tube is attributable to stress corrosion cracking. The susceptibility of the pipe material to SCC was confirmed by the ASTM standard electrochemical reactivation test. About a three orders of magnitude higher anodic current density was measured from the Pyrotherm alloy as compared to 304 SS. The contributors to the SCC are postulated to be sulfur-containing derivatives in the natural gas feedstock and H_2 in the presence of superheated steam under a mechanically-stressed environment. The mechanical stress was produced by bending of the pipe caused by improper suspension design. The likelihood of receiving the largest thermal influx from the burners to the pipe may further accelerate the kinetics of SCC.

Acknowledgements

The authors are grateful to A. Fiedorowicz and R. Henningson for technical assistance, L. Link for the SEM analysis, Dr. H. Li for the XPS analysis and Dr. A. Kapoor for discussion on the steam reforming process.

References

1. R. W. STAEHLE, A. J. FORTY and D. VAN ROOYEN (eds.), Proc. Conf. of Fundamental Aspects of Stress Corrosion Cracking, NACE **1**, (NACE, Houston, TX, 1969).
2. Proc. Conf. on Stress Corrosion Cracking and Hydrogen Embrittlement of Iron Base Alloys, edited by R.W. Staehle, J. Hockmann, R.D. McCright and J.E. Slater, NACE **5** (NACE, Houston, TX, 1977).
3. R. M. LATANISION and J. R. PICKENS (eds.), "Atomistics of Fracture" (Plenum Press, New York, 1983).
4. R. P. SANGLOFF and M. B. IVES (eds.), "Environment-Induced Cracking of Metals," NACE **10**, (NACE, Houston, TX, 1990).
5. S. M. BRUEMMER, E. I. MELETIS, R. H. JONES, W. W. GERBERICH, F. P. FORD and R. W. STACHLE (eds.), Parkins Symposium on Fundamental Aspects of Stress Corrosion Cracking (TMS-AIME, Warrendale, PA, 1992).
6. L. L. SHREIR, R. A. JARMAN and G. T. BURSTEIN (eds.), "Corrosion Vol. 1 Metal/Environment Reactions," 3rd Edn (Butterworth-Heinemann, Oxford, 1993) Ch 8
7. R. M. DAVISON, T. DEBOLD and M. J. JOHNSON, in "Metals Handbook- Corrosion of Stainless Steels" 9th Edn (ASM International, Metal Park, OH, 1987) p. 554.
8. W. BALTHASAR, *Int J Energy* **9** (1984) 649.
9. D. E. RIDLER and M. V. TWIGG, in "Catalyst Handbook," 2nd Edn. (Wolfe Publishing Ltd., Frome, England, 1989) pp 225–80.
10. T. JOHANSEN, K. S. RAGHURAMAN and L. A. HACKETT, *Hydrocarbon Processing* **August** (1992), 119.
11. "Materials Technology in Steam Reforming Processes," Proceedings of the Materials Technology Symposium held at Billingham, U.K. on October 21–22, 1964, edited by C. Edeleanu, (Pergamon Press, New York, 1966).
12. W. STEINKUSCH, Pose-Marre Edelstahlwerk GMBH, Erkrath, Germany (private communications, 1995).
13. "Standard Test Method for Electrochemical Reactivation (EPR) for Detecting Sensitization of AISI Type 304 and 304L Stainless Steels, ASTM G 108 (American Society for Testing and Materials, Philadelphia, PA, 1994).
14. W. STEINKUSCH, *Werkstoffe und Korrosion* **38** (1987) 485.
15. JOHN JONES, Paralloy Limited, Billingham, England (private communications, 1995).
16. L. L. SHREIR, R. A. JARMAN and G. T. BURSTEIN (eds.), in "Corrosion Vol. 1 Metal/Environment Reactions," 3rd Edn (Butterworth-Heinemann, Oxford, 1993) p 7.
17. O. KUBASCHEWSKI and C. B. ALCOCK, "Metallurgical Thermochemistry," 5th Edn (Pergamon Press, New York, 1979) p. 379.
18. R. M. BRICK, A. W. PENSE and R. B. GORDON, "Structure and Properties of Engineering Materials," 4th Edn (McGraw-Hill, New York, 1977) p. 353.
19. D. S. CLARK and W. R. VARNEY, "Physical Metallurgy for Engineers," 2nd Edn (D. Van Nostrand Co., New York. 1962) p. 340.

Received 10 August 1995
and accepted 13 June 1996